Science Advances

AAAS

advances.sciencemag.org/cgi/content/full/4/3/eaar7180/DC1

Supplementary Materials for

Critical advancements in achieving high power and stable nonprecious metal catalyst–based MEAs for real-world proton exchange membrane fuel cell applications

Dustin Banham, Takeaki Kishimoto, Yingjie Zhou, Tetsutaro Sato, Kyoung Bai, Jun-ichi Ozaki, Yasuo Imashiro, Siyu Ye

Published 23 March 2018, *Sci. Adv.* **4**, eaar7180 (2018)
DOI: 10.1126/sciadv.aar7180

This PDF file includes:

Supplementary Text

Gas sorption and Transmission Electron Microscopy

The gas sorption analysis (fig. S5, table S3) reveals that CA#1 is 90 % microporous (with a total surface area of 1100 m^2/g, and a micropore area of 990 m^2/g). Assuming the active sites are housed in micropores, this suggests a relatively high density of active sites. XPS was also used to characterize the chemical composition of the CA#1 (table S1), showing that the catalyst is primarily composed of carbon, oxygen, and nitrogen, with trace Fe, as expected for this family of Fe/N/C NPMC. The XPS spectra reveals three peaks with binding energies of 398.3, 399.8, 400.6, 401.7, and 404.1 eV, respectively, for this sample, which can be assigned to pyridinic-type, Fe-Nx-type, pyrolic-type, quaternary-type, and oxides and graphitic-type nitrogen functional groups. The pyridinic nitrogen constituted less than 20% of the total N1s signals.

TEM images were taken of the catalyst (fig. S6). These images show the presence of some metallic Fe clusters which have also been identified by other researchers in this field. It is believed these Fe clusters are protected by thin graphitic layers, as they would otherwise be dissolved during the acid-wash treatment performed by Nisshinbo. The higher magnification images show defects and exposed edge sites on the catalyst surface, possibly due to the use of Fe in the synthesis of CA#1 which is known to catalyze the formation of defect sites .

Verification of Catalyst Loadings

Prior to performing polarization analysis, it was first important to confirm that a linear correlation exists between the expected catalyst loading and the measured double layer charge for each design. Such a correlation would indicate that the same fraction of catalyst surface is accessible, regardless of loading. Additionally, this provides in-situ verification that the expected differences in loadings were actually achieved. As shown in fig. S1 and table S1, good agreement between the measured and expected trend in double layer charge vs. loading was observed. This provides high confidence that the loadings were in the correct proportions, and that no additional catalyst accessibility limitations occurred for the higher loading designs in the studied loading range.

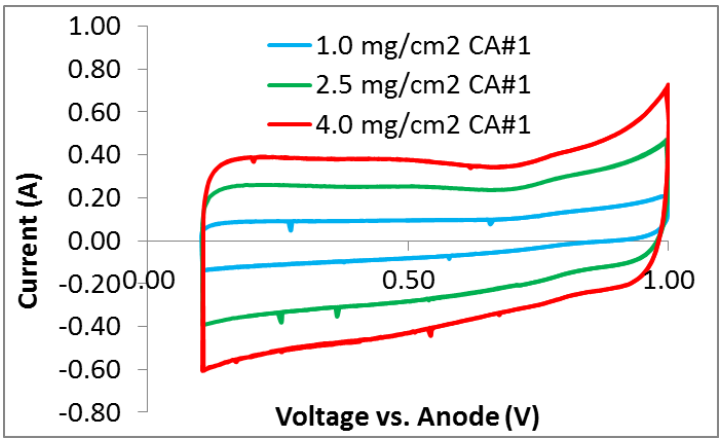

fig. S1. In situ CVs obtained for three different loadings of CA#1. CVs were obtained at 75°C, 120% RH.

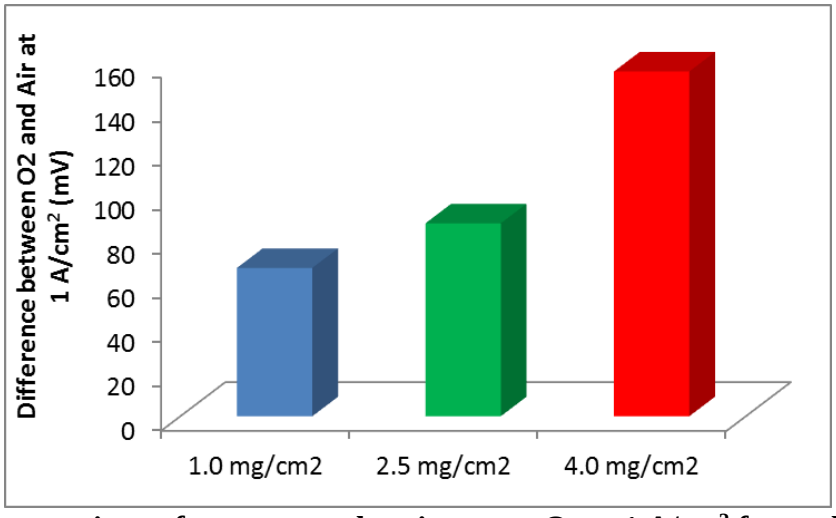

fig. S2. Difference in performance under air versus O_2 at 1 A/cm^2 for each of the three designs.

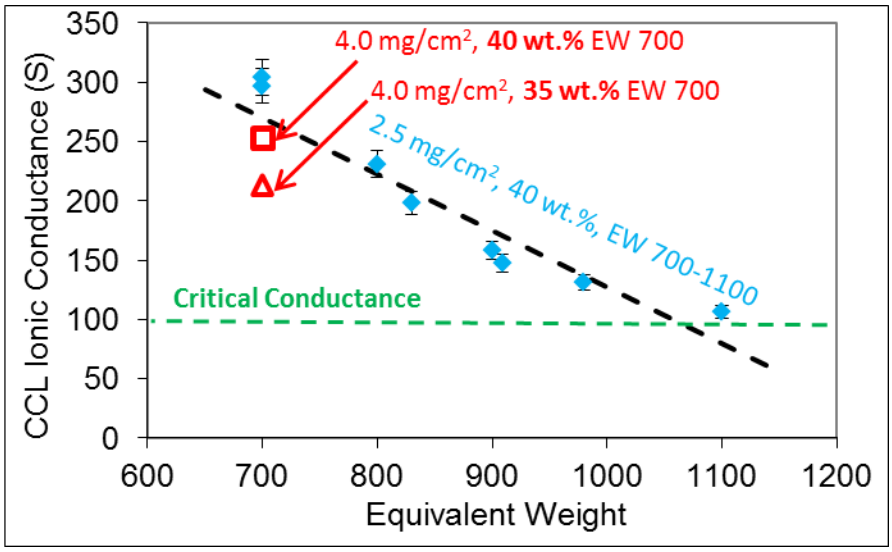

fig. S3. CCL conductance versus ionomer EW.

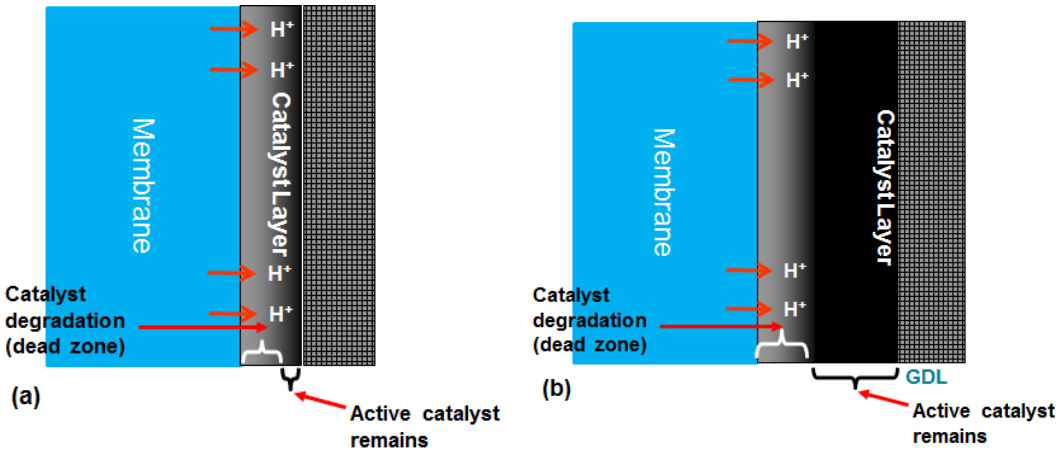

fig. S4. Schematic depiction of how CCL degradation may be expected to proceed in the case of attack by H_2O_2. Since the catalyst adjacent to the membrane is most heavily involved in the ORR, it likely also generates the most H_2O_2. For thin CCLs, this would result in a higher percentage of total catalyst degradation than for thick CCLs.

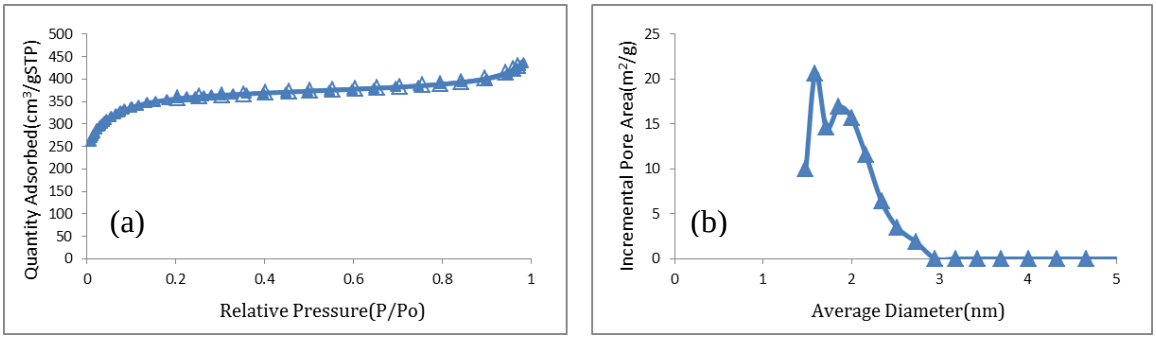

fig. S5. N_2 gas sorption analysis of CA#1. (**a**) N_2 sorption isotherm and (**b**) pore size distributions for CA#1

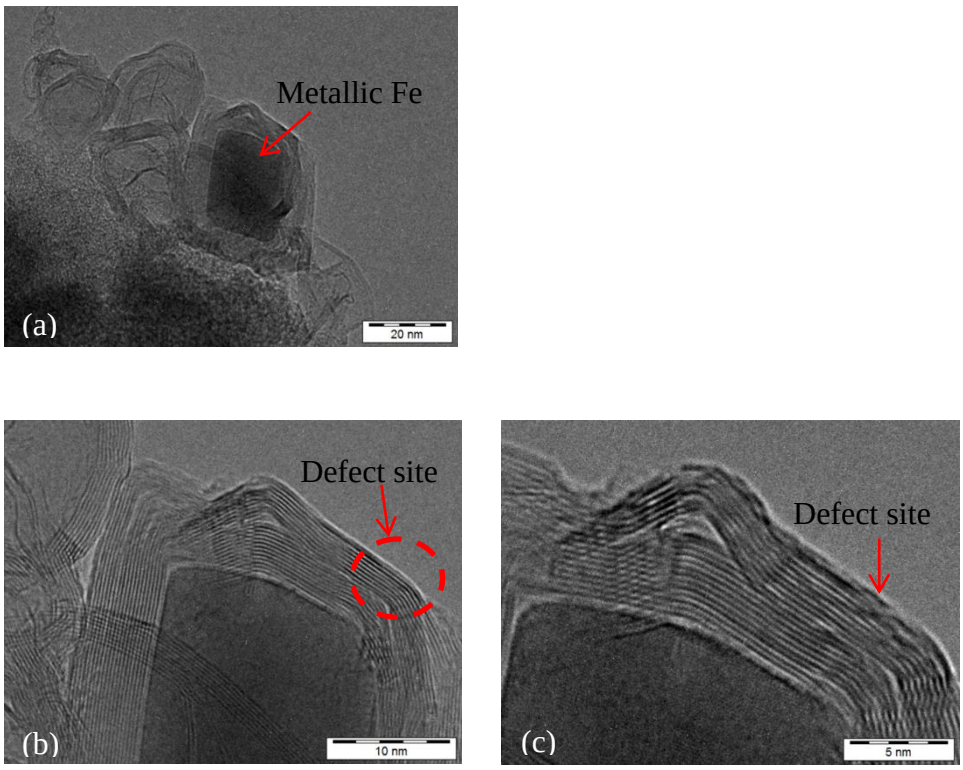

fig. S6. Transmission electron microscopy images of CA#1 obtained at various magnifications.

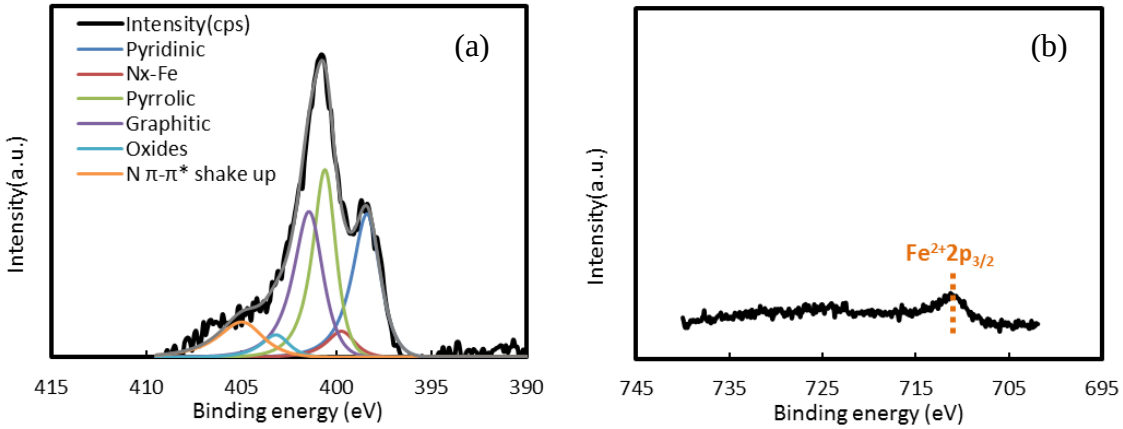

fig. S7. X-ray photoelectron spectroscopy characterization of CA#1. (**a**) N1s and (**b**) Fe2p X-ray photoelectron spectroscopy spectra of CA#1

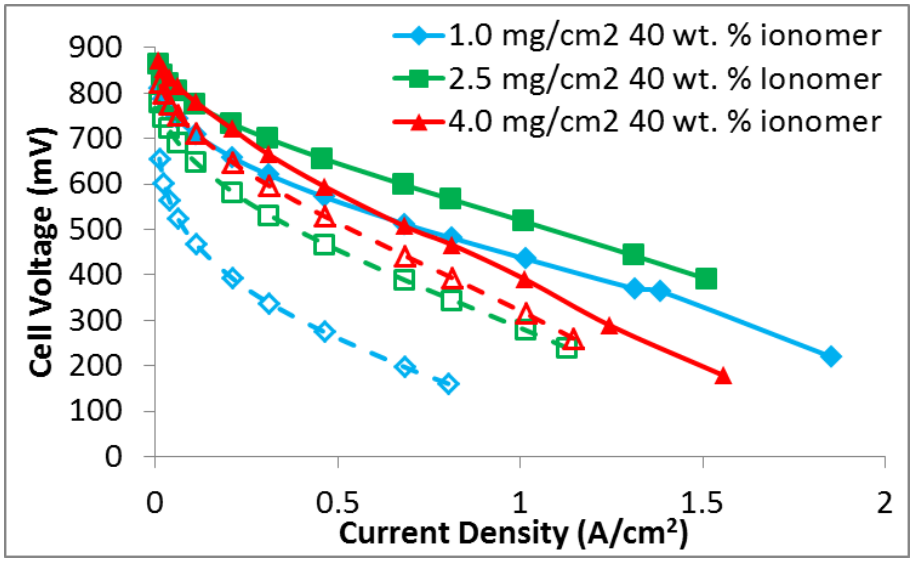

fig. S8. Polarization curves at beginning of test (BOT) (solid lines) and end of test (EOT) (dashed lines) for MEAs prepared from the three different catalyst loadings. Beginning of life (BOL) and end of test (EOT) polarization curves for a) 1.0 mg/cm^2, diamonds, b) 2.5 mg/cm^2, squares, and c) 4.0 mg/cm^2, triangles. BOL curves are shown by a solid line, and EOT curves are shown by a dashed line.

table S1. Double-layer charge normalized to the charge obtained for the 1.0 mg/cm^2 design.

	Charge normalized to 1.0 mg/cm^2
1.0 mg/cm^2	1.00
2.5 mg/cm^2	2.82
4.0 mg/cm^2	4.28

table S2. XPS characterization of CA#1.

Atomic Conc.(%)					
C 1s	O 1s	N 1s	Fe (2p)	N/C（%）	O/C(%)
90.96	7.12	1.62	0.21	1.78	7.82

table S3. Gas sorption analysis.

	BET surface area (m^2/g)	Total pore volume (cm^3/g)	Micropore Area (m^2/g)
CA#1	1085	0.67	991

table S4. Fe and Zn content based on inductively coupled plasma measurements of CA#1.

	Fe(wt%)	Zn(wt%)
CA#1	0.88	0.00